Presented at the 26th European PV Solar Energy Conference and Exhibition, 5-9 September 2011, Hamburg, Germany

QUALITY CONTROL OF CZOCHRALSKI GROWN SILICON WAFERS IN SOLAR CELL PRODUCTION USING PHOTOLUMINESCENCE IMAGING

Jonas Haunschild, Juliane Broisch, Isolde E. Reis, Stefan Rein
Fraunhofer Institute for Solar Energy Systems
Heidenhofstrasse 2, 79110 Freiburg im Breisgau, Germany
Phone: +49 761-4588-563, fax: +49 761-4588-9250
E-Mail: jonas.haunschild@ise.fraunhofer.de

ABSTRACT: Recent progress with photoluminescence (PL) imaging shows that applying pattern recognition techniques on the images of as-cut multicrystalline silicon (mc-Si) wafers allows a prediction of final solar cell parameters. Based on PL a reliable quality control for electrical parameters can thus be established for mc-Si wafers. High-efficiency solar cells are fabricated from Czochralski silicon (Cz-Si) wafers in most cases because of their high material quality. In this study, however, solar cells from Cz-Si suffered an efficiency loss of more than 4 % absolute due to a defect which appears as dark rings in PL images. In this paper we will show that the origin of this defect lies in oxygen precipitation during emitter diffusion. By using QSSPC-based lifetime measurements or PL-imaging, critical wafers can be identified and sorted out reliably at an early state of production and thus yield and average efficiency of production lines can be increased.
Keywords: Defects, Characterization, Photoluminescence

1 INTRODUCTION

Only six years after T. Fuyuki [1] and T. Trupke [2] have proposed electro- and photoluminescence imaging (EL, PL) as characterization tools for solar cells and wafers, these techniques has since become widely used. The yearly market survey of PHOTON [3] shows an increasing number of companies selling EL tools. Also concerning PL, new companies enter the market. The success of luminescence imaging lies in the fact of being a very fast and non-destructive characterization technique for electrical parameters with high spatial resolution [4, 5]. Defects do not appear as a single value, but as a pattern in the images. If known which defect causes which specific pattern, the images can be interpreted and thus a more precise quality control and process development can be performed [6].

One of the most promising applications for PL-imaging is the incoming quality control (IQC) of multicrystalline silicon (mc-Si) wafers in the as-cut state. In IQC all wafers whose mechanical or electrical quality is not sufficient for producing high performance solar cells, should be rejected or sorted into an adequate production process. Due to the surface damage of as-cut wafers, bulk lifetime information is highly masked and therefore almost invisible to state of the art characterization tools. Approaches to overcome this issue are currently under research [7, 8]. The limited lifetime information is also an issue for PL imaging, but fortunately most electrical defects which are formed during crystallization, appear as very distinct pattern in PL images. By applying pattern recognition, it has been shown that open circuit voltage, short circuit current and efficiency can be predicted for a known solar cell process [9, 10]. Current research aims on establishing a reliable wafer rating based on an automatic evaluation of PL images which can be acquired with high resolution in inline speed.

Material quality of Czochralski grown silicon (Cz-Si) is much higher compared to mc-Si. Therefore the focus of IQC using PL imaging was laying on mc-Si so far. However, recent studies showed that also in Cz-Si wafers significant differences in material quality can be present [11, 12]. Especially when using Cz-Si wafers for high efficiency solar cell concepts exceeding 20 % efficiency, minor defects can limit cell performance [13]. Please note that in this study the focus does not lie on the metastable defect formed by boron-oxygen pairing (BO) [14, 15] but on more severe background defects.

2 OXYGEN RELATED DEFECTS IN CZ-SI

Oxygen-related defects in Cz-Si have been characterized thoroughly for semiconductor devices [16, 17], while the question of how these defects influence solar cells is of increasing importance as highly efficient solar cell concepts rely on very pure material. Typical oxygen concentrations in Cz-Si are in the range of 10^{17}-10^{18} cm^{-3}. Primarily it enters into the silicon melt through outdiffusion from the quartz crucible and is build into the silicon lattice during crystallization. Depending on temperature and pulling speed during crystallization, interstitial- or vacancy-rich regions can form which assist precipitation and formation of oxygen defects differently [18]. The variety of these defects is large and the influence on carrier lifetime varies. Some can be activated by high-temperature steps and some are deactivated, depending on the plateau temperatures and the heating and cooling ramps of high-temperature steps during solar cell processing. The most prominent defects are thermal donors [19, 20] which strongly influence resistivity measurements and the boron-oxygen-complex [14, 15] which leads to degradation effects of the final solar cells.

In semiconductor physics oxygen precipitation is another well-known effect [21, 22], which may lead to severe defects which can cause failure of integrated circuits. Applying a special thermal treatment during production their growth can be controlled to take place only in the bulk where they getter impurities from the surface and thus even increase material quality. In photovoltaics both bulk and surface need to be free of precipitates. Only recently formation of oxygen precipitates has been investigated with focus on solar cells [23]. In this paper we will evaluate their influence during solar cell production and how to detect them using inline tools.

3 EXPERIMENTAL

The definitions for the Cz-Si IQC, presented in this paper, are based on a broad material evaluation using wafers from different crystal positions, manufacturers and crystallization processes. 200 wafers with resistivities specified from 1 – 6 Ωcm were grouped according to their appearance in the PL image of the as-cut state. Half of the wafers were processed using a standard 156 x 156 mm^2 solar cell process including alkaline texturing, two sided emitter diffusion, phosphorus silicate glass etching, anti-reflection-coating, screen-printing, fast firing and laser edge isolation. The other half of the wafers consisting of adjacent wafers to the processed wafers was used for a more detailed characterization. Solar cells whose efficiency was limited by process-induced defects such as shunts or high series resistances have been identified by applying thermographical measurements and quantitative PL imaging [24] and were excluded from this study to focus only on material-related issues.

PL imaging was performed on the setup build at Fraunhofer ISE where a laser at 790 nm irradiates the sample area with an illumination equivalent of up to two suns. The radiative band-to-band recombination of the excited charge carriers is detected using a Si-CCD camera with appropriate filters mounted in front of the camera lens to block reflected excitation light.

4. EFFICIENCY LIMITING DEFECTS IN CZ-SI SOLAR CELLS

4.1 Solar cell characteristics

The results from IV-curve measurements reveal that the efficiency ranges from 14.4 % up to 18.4 % in the non-degraded state. In figure 1, PL images of a lowly efficient and a highly efficient solar cell are shown. As process-related problems can be excluded, efficiency is limited by the ring-like defect structure, which is highly recombination-active and thus appears dark in the PL image in figure 1b. The observed efficiency drop by 4 % (absolute) can thus be attributed to poor material quality.

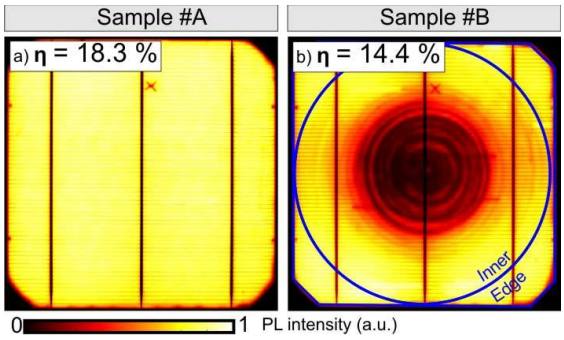

Figure 1: PL images of two finished solar cells. Sample #A resulted in 18.3% efficiency and shows no rings, while sample #B resulted in only 14.4 % and shows strong rings.

4.2 Ring defect strength (RDS) and correlations

In order to find out if the differences in efficiency scale with the intensity of the rings visible in PL images, we set up a simple metric in which the mean count rates of the edge region is divided by the mean count rates of the inner region of the luminescence signal under open circuit conditions marked in figure 1b. Both regions are symmetric to the center of the solar cells. The position of the circle was chosen to cover the largest extension of rings in this study and is applied to all solar cells. Please note that this procedure is only feasible if the PL image is not covered completely by rings.

$$RDS = \frac{< I_{PL}(x,y) >|_{Edge}}{< I_{PL}(x,y) >|_{Inner}} \qquad (1)$$

Figure 2 shows the correlation of the ring defect strength to the solar cell efficiency with a correlation coefficient of $R^2 = 0.94$. Thus the loss of efficiency in this batch can clearly be attributed to material defects within the Cz-Si wafers which appear as concentric ring like defect pattern in the PL images.

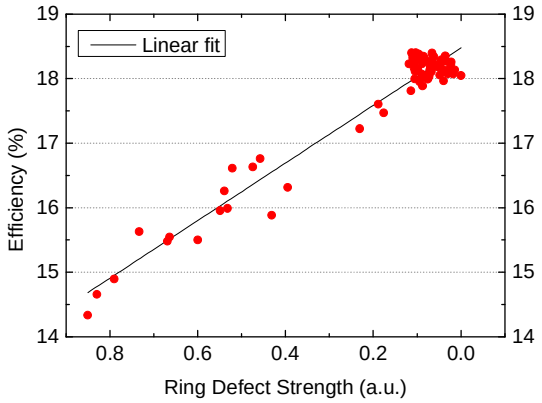

Figure 2: Solar cell efficiency as a function of the ring defect strength (defined as ratio of the average PL-intensities in the centre and the edge region displayed in fig. 1) measured at the finished Cz-Si solar cells.

It should be stressed that the material used here was taken from commercial available material labeled to be "high quality". The difference in efficiencies of more than 4 % absolute is not tolerable for industrial solar cell processing. Especially high efficiency solar cell concepts are expected to suffer even more if material quality limits the efficiency to below 15 %. Now two questions arise: i) can these defects be detected in early stages of production so that a reliable IQC allows concerned wafers to be directly rejected and ii) what is its physical origin?

5. DEFECT CHARACTERISTICS IN DIFFERENT PRODUCTIONS STATES

5.1 As-cut characteristics

Characterizing Cz-Si wafers by PL, their image is expected to look homogeneous, because there should be no major material defects present. However a random sampling from wafers from the storage at Fraunhofer ISE revealed different kinds of ring- and swirl-structures. Four representative samples are displayed in figure 3 in addition with their solar cell efficiency. Images a) and b) are the same samples as in figure 1 (here in as-cut state). Although they resulted in very different efficiencies, the PL images both show rings of medium intensity. Sample #C looks homogeneous, as do most PL images of Cz-Si as-cut wafers and resulted in a high efficiency. Image d)

shows bright edges with the center yielding almost no signal while the final solar cell surprisingly has a high efficiency.

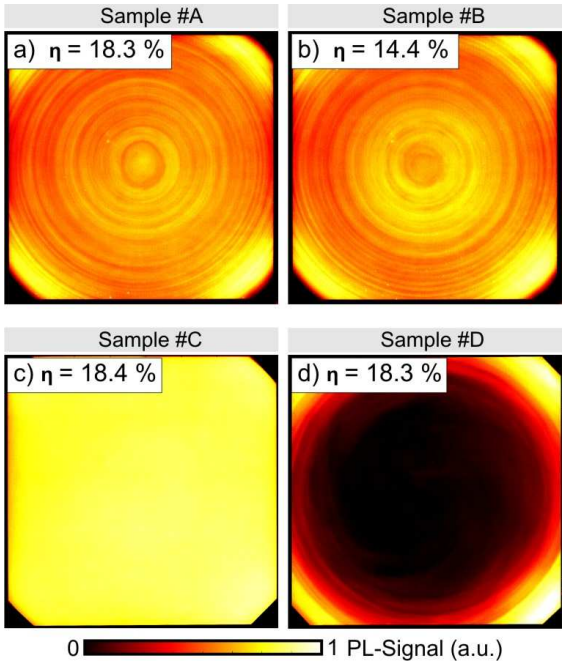

Figure 3: PL images of Cz-Si as-cut wafers: c) a typical homogeneous image, while a), b) and d) show different kinds of ring patterns. The rings are caused by lateral differences in lifetime and doping. The efficiencies represent the values of the finished solar cells processed from these wafers.

All wafers in this batch can be sorted in one of the four groups having a similar PL image as in figure 3. Group A shows medium rings resulting in high solar cell efficiency. Group B is the one which we focus on also having medium rings but resulting in low efficiency. Wafers from group C show no rings and result in high efficiency while group D wafers have strong rings but also results in highly efficient solar cells. It would be desirable to identify wafers with too low material quality (group B) during incoming inspection to be able to directly reject these wafers or to transfer them to specially adjusted production lines. Figure 3 shows that this is not possible only by using PL imaging as groups A and B yield the same ring pattern.

In figure 4a, solar cell efficiency is plotted as a function of the effective charge carrier lifetime measured on the individual wafers in the as-cut state using the quasi-steady state photoconductance (QSSPC) technique. With the inline-setup used, the measurement is performed on a coil of 55 mm diameter in the center of the wafer and the lifetime values are extracted at an injection density $\Delta n = 5\times10^{14}$ cm^{-3}. In the graph the four groups are marked. For wafer groups A and C with as-cut lifetimes in the range of 0.7 µs the small differences in carrier lifetime do not correlate to small differences in cell efficiency. In this case the lifetime in the finished cell obviously is high enough to reach the efficiency limit of the process. For group B with as-cut lifetimes in the same range, cell efficiency varies strongly from 14.4 % to 17.6 %, which is not reflected in lifetime in the as-cut state. Group D wafers with high as-cut lifetimes above 1.0 µs did not result in higher efficiencies.

In figure 4b trap density extracted according to Ref. [8] shows that the lifetime values of group D are increased by trapping artifacts which cannot be completely removed in spite of a trapping correction, while wafers from groups A-C are not affected by trapping.

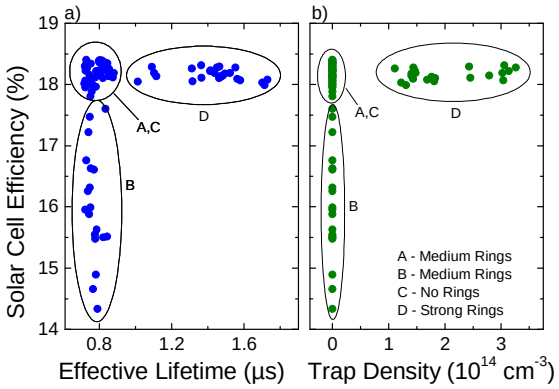

Figures 4: Solar cell efficiency (a) as a function of effective carrier lifetime, measured by means of QSSPC on the as-cut wafers and (b) as a function of trap density. Lifetime is limited by surface recombination and superimposed by charge carrier trapping which may be corrected.

Beside PL-imaging also lifetime measurements and the investigation of trap density do not allow do distinguish between groups A and B. This behavior is caused either by the surface limitation of carrier lifetime or by a defect activation at a later process stage. If this is the case the harmful effect from group B may not be detected unambiguously in the as-cut state. Further research is required.

5.2 Check for thermal donors

An inline measurement of the base resistance yields values between 1.19 - 82.7 Ωcm, which is out of the specification of the material (1 – 6 Ωcm). Increased and inhomogeneous resistance values on as-cut wafers are caused by the well known defect of thermal donors (TD) in most cases. TD can be destroyed in a high temperature step (e.g. emitter diffusion) and should have no effect on final solar cell results. In figure 5 the results of an inline test before and after a thermal treatment which was performed in an inline furnace with a peak temperature of 800°C for 10 seconds are plotted. After the treatment all TD were dissolved and resistivity was in the expected range for all tested wafers. The graph shows the absolute reduction in resistivity upon annealing plotted against the solar cell efficiency. If no rings in the PL images are present (group C), the resistivity of the wafers does not change significantly. Wafers from groups A and B change from 1- 10 Ωcm, while for group D the change is more than 10 Ωcm. So we can attribute: Group A, B have weak TD, group C has no TD and group D has strong TD.

While groups A and B cannot be distinguished by their change in resistivity, the rings in the PL images of group A vanish, while they get stronger for group B. The same effect occurs upon emitter diffusion and is discussed in the following section.

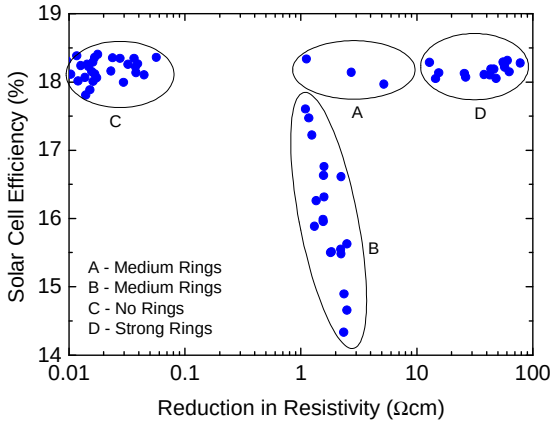

Figure 5: Reduction in resistivity upon annealing plotted against the solar cell efficiency. Wafers from group C show the noise of the measurement while resistivities of groups A, B and D are reduced by more than 1 Ωcm.

5.3 Characterization after emitter diffusion

Figure 6 shows the PL images from figure 3 in the as-cut state and the PL images of the same wafers after emitter diffusion. Wafers from group A result in homogeneous PL images, leading to the conclusion the ring effect in the as-cut state was caused by weak thermal donors. Wafers from group B, however, result in a PL image with a dark center of low lifetime. In addition to weak thermal donors a more severe background defect must be present which is activated during high temperature processing. Group C wafers show no change, while the very dark rings of group D vanish. Therefore strong rings in PL images of as-cut wafers can be attributed to strong but harmless thermal donors.

Figure 7 shows the solar cell efficiencies plotted as a function of (a) the effective lifetime obtained from inline QSSPC and (b) the ring defect strength extracted from PL

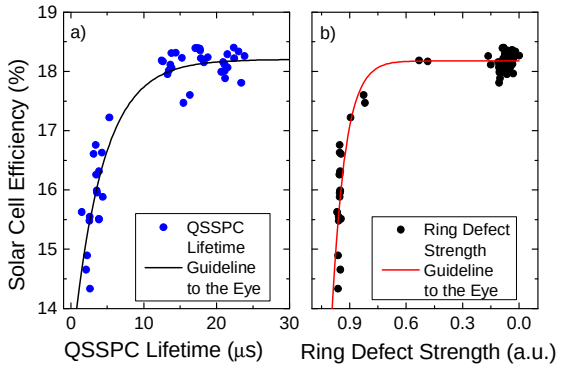

Figure 7: Solar cell efficiency plotted against QSSPC lifetime and PL ring defect strength, respectively, both measured after emitter diffusion. With both methods wafers resulting in low efficiency can be identified reliably.

images, both quantities measured after emitter diffusion. While low efficiencies can obviously be attributed to low carrier lifetimes, the solar cell process limits cell efficiency above approx. 20 µs. The PL ring defect strength evaluation yields similar results and confirms that the low lifetimes originate from ring features. Therefore, both methods can be used for a wafer rating after emitter diffusion.

6 DEFECT CHARACTERIZATION

To shed some light on the physical origin of the observed defect structures, a more detailed defect characterization has been performed on adjacent wafers for selected material types. Using infrared transmission (FTIR) the interstitial oxygen content was measured on samples with ring defects after emitter diffusion. For a wafer

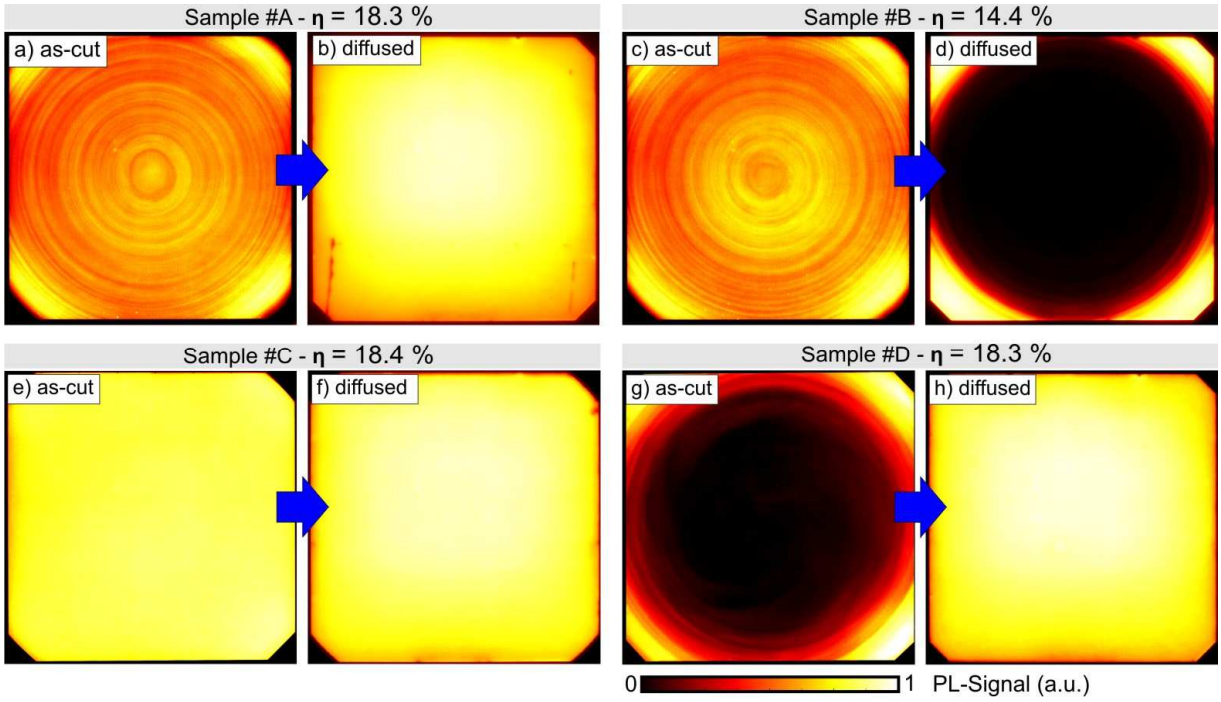

Figure 6: PL images of the as-cut wafer (same as in fig. 3) are displayed left and PL images of the same wafers after emitter diffusion are displayed right. While for samples #A and #D the rings vanish, they become stronger for sample #B.

comparable to sample #C (without rings) the interstitial oxygen concentration was measured with O_i=7x10^{17} cm^{-3} and for a wafer comparable to sample #B (with rings) O_i=1x10^{17} cm^{-3} was measured. That the sample with ring defects has a lower interstitial oxygen concentration indicates that more oxygen precipitates could be present which cannot be measured by means of a simple FTIR analysis.

In order to prove the presence of oxygen precipitates, the samples were polished and wet chemically etched using the Sirtl-etch [25]. Figure 8a shows the PL image of sample #C and in figure 8b-d the microscope pictures of small areas of the same sample can be seen. Apart from dust particles and a scratch, no precipitates are present. Figure 9a shows the PL image of sample #B with ring defects. For this sample the images of the optical microscope (see fig. 9b-d) reveal that in the outer region of the wafer with high PL-signal no precipitates are present, while in the inner region with low PL signal lots of precipitates can be found. Thus we find that the drop in lifetime and efficiency of group B can be attributed to the presence of oxygen precipitates.

7 CONCLUSION

In this study it is shown that in commercially available Cz-Si materials, labelled as “high quality”, oxygen precipitates can occur which might reduce solar cell efficiency by more than 4 % (absolute). This defect appears as dark concentric rings in PL images throughout the production process. Detection of oxygen precipitates in the as-cut state during incoming inspection is rather difficult as the presence of harmless thermal donors can form similar patterns. Only if the presence of thermal donors can be excluded, detection of wafers which form oxygen precipitates during emitter diffusion might be possible using PL-imaging in incoming inspection. If thermal donors cannot be excluded, reliable quality control is possible after emitter diffusion using lifetime measurements or PL imaging, respectively. Using these results a PL-imaging based IQC was introduced into the PV-TEC production lab at Fraunhofer ISE.

8 ACKNOWLEDGEMENT

We thank Martin Schubert for fruitful discussions. This work has been supported by the Fraunhofer Society under the frame of the project ABICS-LUM.

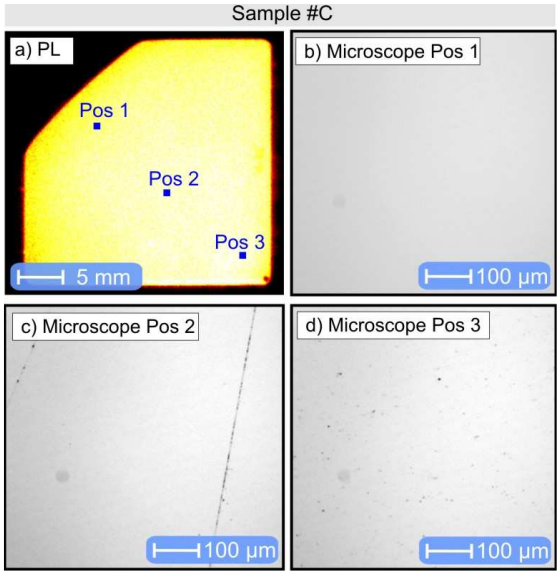

Figure 8: PL image of sample #C (a) after preferential etching. Optical microscope pictures (b-d) of the marked positions; no precipitates can be observed.

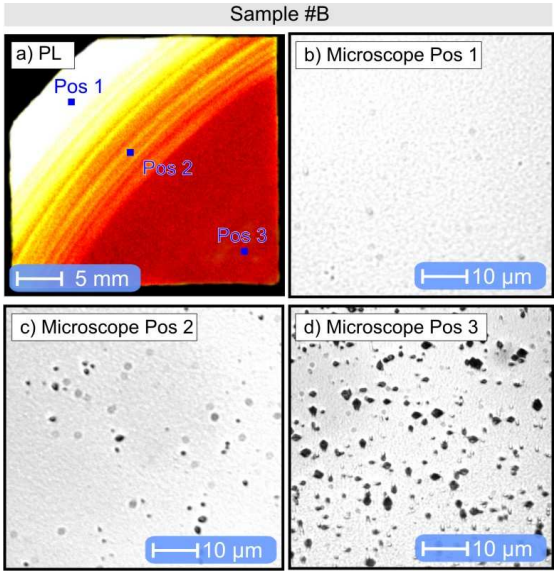

Figure 9: PL image of sample #B (a) after preferential etching. Optical microscope pictures (b-d) of the marked positions; the darker the PL image, the more precipitates can be found.

9 REFERENCES

[1] T. Fuyuki, H. Kondo, T. Yamazaki, et al., Applied Physics Letters 86 (2005) 262108/1.
[2] T. Trupke, R.A. Bardos, M.C. Schubert, et al., Applied Physics Letters 89 (2006) 44107.
[3] S.K. Chunduri, Photon International 01 (2011) 158.
[4] H. Nagel, Proceedings 20th Workshop on Crystalline Silicon Solar Cells & Modules, Breckenridge, Colorado, USA (2010) 40.
[5] T. Trupke, J. Nyhus, & J. Haunschild, Physica Status Solidi RRL 5 (2011) 131–137.
[6] J. Haunschild, M. Glatthaar, M. Demant, et al., Solar Energy Materials and Solar Cells 94 (2010) 2007.
[7] K. Bothe, R. Krain, R. Brendel, et al., Proceedings of the 25th EU-PVSEC, Valencia, Spain (2010) 204.
[8] R. Sinton, J. Swirhun, M. Forsyth, et al., Proceedings of the 25th EU-PVSEC, Valencia, Spain (2010).
[9] W. McMillan, T. Trupke, & J.W. Weber, Proceedings of the 25th EU-PVSEC, Valencia, Spain (2010) 1346.
[10] M. Demant, J. Haunschild, M. Glatthaar, et al., Proceedings of the 25th EU-PVSEC, Valencia, Spain (2010) 1078.
[11] A. Lawerenz, K. Lauer, M. Blech, et al., Proceedings of the 25th EU-PVSEC, Valencia, Spain (2010) 2486.

[12] J. Haunschild, J. Geilker, I.E. Reis, et al., Physica Status Solidi RRL 5 (2011) 199.
[13] P.J. Cousins, D.D. Smith, H.-C. Luan, et al., Proceedings of the 35th IEEE PVSC, Honolulu, Hawaii, USA (2010) 000275.
[14] S. Rein, T. Rehrl, W. Warta, et al., Proceedings of the 17th EU-PVSEC, Munich, Germany (2001) 1555.
[15] J. Schmidt, & K. Bothe, Physical Review B (Condensed Matter) 69 (2004) 0241071.
[16] K. Marsden, T. Kanda, M. Okui, et al., Materials Science and Engeneering B 36 (1996) 16.
[17] M. Porrini, P. Collareta, G. Borionetti, et al., Materials Science and Engineering B 37 (2000) 139.
[18] V.V. Voronkov, & R. Falster, Journal of Crystal Growth 204 (1999) 462.
[19] N. Meilwes, J.-M. Spaeth, W. Gotz, et al., Semiconductor Science and Technology 9 (1994) 1623.
[20] P. Wagner, & J. Hage, Applied Physics A 49 (1989) 123.
[21] A.J.R. De Kock, P.J. Roksnoer, & P.G.T. Boonen, Journal of Crystal Growth 28 (1975) 125.
[22] H. Föll, Applied Physics A 8 (1975) 319.
[23] L. Chen, X. Yu, P. Chen, et al., Solar Energy Materials & Solar Cells 95 (2011) 3148.
[24] M. Glatthaar, J. Haunschild, M. Kasemann, et al., Physica Status Solidi RRL 4 (2010) 13.
[25] E. Sirtl, & A. Adler, Z. Metallkde. 52 (1961) 529.